J Physiol 587.19 (2009) pp 4661–4680

The Journal of Physiology

Origin of complex behaviour of spatially discordant alternans in a transgenic rabbit model of type 2 long QT syndrome

Ohad Ziv[1], Eduardo Morales[1], Yoon-kyu Song[2], Xuwen Peng[3], Katja E. Odening[1], Alfred E. Buxton[1], Alain Karma[4], Gideon Koren[1] and Bum-Rak Choi[1]

[1]*Cardiovascular Research Center, Division of Cardiology, Rhode Island Hospital, Warren Alpert Medical School of Brown University, Providence, RI, USA*
[2]*Engineering Division, Brown University, Providence, RI, USA*
[3]*Department of Comparative Medicine, Pennsylvania State University College of Medicine, Hershey, PA, USA*
[4]*Northeastern University, Department of Physics, Boston, MA, USA*

Enhanced dispersion of repolarization has been proposed as an important mechanism in long QT related arrhythmias. Dispersion can be dynamic and can be augmented with the occurrence of spatially out-of-phase action potential duration (APD) alternans (discordant alternans; DA). We investigated the role of tissue heterogeneity in generating DA using a novel transgenic rabbit model of type 2 long QT syndrome (LQT2). Littermate control (LMC) and LQT2 rabbit hearts ($n = 5$ for each) were retrogradely perfused and action potentials were mapped from the epicardial surface using di-4-ANEPPS and a high speed CMOS camera. Spatial dispersion (ΔAPD and Δslope of APD restitution) were both increased in LQT2 compared to LMC (ΔAPD: 34 ± 7 ms *vs.* 23 ± 6 ms; Δslope:1.14 ± 0.23 *vs.* 0.59 ± 0.19). Onset of DA under a ramp stimulation protocol was seen at longer pacing cycle length (CL) in LQT2 compared to LMC hearts (206 ± 24 ms *vs.* 156 ± 5 ms). Nodal lines between regions with APD alternans out of phase from each other were correlated with conduction velocity (CV) alternation in LMC but not in LQT2 hearts. In LQT2 hearts, larger APD dispersion was associated with onset of DA at longer pacing CL. At shorter CLs, closer to ventricular fibrillation induction (VF), nodal lines in LQT2 ($n = 2$ out of 5) showed persistent complex beat-to-beat changes in nodal line formation of DA associated with competing contribution from CV restitution and tissue spatial heterogeneity, increasing vulnerability to conduction block. In conclusion, tissue heterogeneity plays a significant role in providing substrate for ventricular arrhythmia in LQT2 rabbits by facilitating DA onset and contributing to unstable nodal lines prone to reentry formation.

(Received 6 May 2009; accepted after revision 6 August 2009; first published online 10 August 2009)
Corresponding author B.-R. Choi: Cardiovascular Research Center, Rhode Island Hospital and Warren Alpert Medical School of Brown University, Providence, RI 02903, USA. Email: bum-rak_choi@brown.edu

Abbreviations AI, activation interval; APA, action potential amplitude; APD, action potential duration; CL, cycle length; CV, conduction velocity; DA, discordant alternans; DI, diastolic interval; EAD, early afterdepolarization; *F*, fluorescence; LMC, littermate control; LQT, long QT; LQTS, long QT syndrome; LQT2, type 2 long QT syndrome; LV, left ventricle; RV, right ventricle; SCD, sudden cardiac death; VF, ventricular fibrillation; VT, ventricular tachycardia.

Congenital long QT syndrome (LQTS) is a familial disease, characterized by prolongation of the QT interval on surface ECG and sudden cardiac death caused by polymorphic ventricular tachycardia (VT) (Dessertenne, 1966; El-Sherif & Turitto, 1999; Schwartz, 2006; Saenen & Vrints, 2008). Twelve different genes have been found to be associated with LQTS (Morita *et al.* 2008; Webster & Berul, 2008) but in the vast majority of successfully genotyped patients, the underlying causes are mutations in the voltage-gated potassium channels. Long QT syndrome type 2 (LQT2) is one of the most common and arrhythmogenic forms of long QT syndrome (Sauer *et al.* 2007) caused by a mutation in the *KCNH2* gene which encodes the HERG polypeptide, the α subunit of the rapid component of delayed rectifier potassium currents I_{Kr}.

© 2009 The Authors. Journal compilation © 2009 The Physiological Society
DOI: 10.1113/jphysiol.2009.175018

LQT related ventricular arrhythmia most likely results from the combination of triggered activity such as early afterdepolarizations (EADs) and enhanced dispersion of repolarization (see review in Liu & Laurita, 2005; Antzelevitch, 2007). Dispersion of repolarization is not static but rather dynamically changing depending on heart rates and autonomic tone. Dispersion can be accentuated when beat-to-beat alternation in action potential duration (APD) exists, known as APD alternans. The cause of APD alternans has been attributed to the cellular properties of APD adaptation to heart rate changes, known as APD restitution (Gettes & Reuter, 1974; Garfinkel, 2007), as well as to calcium transient restitution (Clusin, 2003; Pruvot *et al.* 2004; Goldhaber *et al.* 2005). When APD alternans is spatially out of phase (discordant), with one region in the short APD phase and an adjacent region in the long APD phase, dispersion of repolarization increases dramatically, causing higher vulnerability to reentry formation (Pastore *et al.* 1999; Qu *et al.* 2000).

In LQTS, repolarization alternans on a surface ECG, in the form of T wave alternans, has been associated with life-threatening arrhythmias (Schwartz & Malliani, 1975; Schwartz *et al.* 1975; Zareba *et al.* 1994; Fagundes *et al.* 2000; Schwartz, 2006). In addition, in animal models of drug-induced LQTS, transmural discordant alternans has been demonstrated (Chinushi *et al.* 2003), suggesting discordant alternans (DA) may be involved in LQT related arrhythmias. However, the mechanisms by which DA emerges in long QT syndrome have yet to be specified. In general, three mechanisms have been proposed to explain the onset DA in the heart; heterogeneous APD restitution, conduction velocity (CV) restitution (Qu *et al.* 2000; Hayashi *et al.* 2007; Wilson & Rosenbaum, 2007), and Ca^{2+} handling heterogeneities (Clusin, 2003; Laurita *et al.* 2003; Pruvot *et al.* 2004; Goldhaber *et al.* 2005; Weiss *et al.* 2006; Sato *et al.* 2007; Wilson *et al.* 2009). Understanding the mechanisms of DA in LQT2 and their relation to arrhythmia may improve future risk assessment of sudden cardiac death (SCD) in LQT patients and potentially may contribute to advancement of therapeutic strategies.

The purpose of this study is to investigate mechanisms underlying discordant alternans in LQTS and its relationship to LQT related ventricular arrhythmias. We used a novel transgenic rabbit model of LQT2 created by over-expression of a pore mutant of the human gene *KCNH2* (HERG-G628S) in the rabbit heart (Brunner *et al.* 2008; Odening *et al.* 2008). Unlike typical transgenic mice models, this rabbit model shows an action potential with a plateau similar to the human action potential. Furthermore, this model has demonstrated a high incidence of spontaneous polymorphic VT and sudden cardiac death, thus providing an excellent model for LQT-related arrhythmias. Previously, we demonstrated that the spatial dispersion of APD in LQT2 rabbits is increased across the epicardial surface and that this increased APD dispersion is linked to their arrhythmogenesis (Brunner *et al.* 2008). Therefore, we hypothesized that in this LQT2 model where spatial dispersion is greatly increased compared to controls, spatial heterogeneity will play a key role in the generation of discordant alternans, in contrast to control rabbits where lack of baseline APD dispersion will require conduction velocity alternans to occur in order to produce discordant APD alternans. Using optical mapping techniques, we mapped CV and APD dynamics, and identified in LQT2 rabbits and controls spatially out-of-phase APD alternans (DA) and the nodal lines that divide out-of-phase regions in order to determine the mechanisms underlying the formation of DA and the behaviour of DA nodal lines. Our data emphasize the importance of repolarization heterogeneity in LQT2-related arrhythmias via the formation of DA that results in conduction block.

Methods

Heart preparations

Littermate control (LMC) and transgenic rabbits were injected with buprenorphene ($0.03\,mg\,kg^{-1}$ I.M.), acepromazine ($0.5\,mg\,kg^{-1}$ I.M.), xylazene ($15\,mg\,kg^{-1}$ I.M.), ketamine ($60\,mg\,kg^{-1}$ I.M.), pentothal ($35\,mg\,kg^{-1}$ I.V.) and heparin ($200\,U\,kg^{-1}$). After appropriate level of anaesthesia was obtained as determined by corneal reflex and response to painful stimuli, rabbits were killed via beating heart harvest. To preserve uniformity in our sample and to avoid the potential differences that sex hormones may generate, we chose only male LQT2 and LMC rabbits weighing ~3.5–5.5 kg. Due to shared resources with other investigations, rabbits were obtained and studied from three different litters over a 10 month period. This investigation conformed to the current *Guide for Care and Use of Laboratory Animals* published by the National Institutes of Health (NIH Publication No. 85-23, revised 1996), as well as the standards recently delineated in this journal (Drummond, 2009), and was approved by the Animal Welfare Committee at Rhode Island Hospital.

The heart was excised from the chest and retrogradely perfused through the aorta with (in $mmol\,l^{-1}$) 130 NaCl, 24 $NaHCO_3$, 1.0 $MgCl_2$, 4.0 KCl, 1.2 NaH_2PO_4, 5 dextrose, 25 mannitol, 1.25 $CaCl_2$, at pH 7.4, gassed with 95% O_2 and 5% CO_2. In total, 10 rabbits were studied: littermate control ($n = 5$) and LQT2 ($n = 5$). Temperature was maintained at $37.0 \pm 0.2^{\circ}C$ and perfusion pressure was adjusted to ~60 mmHg with a peristaltic pump (Radnoti Glass Technology, Monrovia, CA, USA). Hearts were placed in a chamber to maintain temperature, and to reduce movement artifact $5\,\mu mol\,l^{-1}$ blebbistatin was added to the perfusate (Fedorov *et al.* 2007).

© 2009 The Authors. Journal compilation © 2009 The Physiological Society

Optical mapping

The optical apparatus has been previously described (Choi *et al.* 2007). Fluorescence images from the anterior surface and LV free wall of heart were focused on a CMOS camera (100 × 100 pixels, Ultima-L, Scimedia, Japan) with a 50 mm Nikon f/1.2 lens which results in the field of view of 1.5 cm × 1.5 cm Fig. 1*A*) with a spatial resolution of 150 μm × 150 μm. Excitation light was illuminated through a dichroic box located between the camera lens and the camera. Sampling rate was set to 1000 frames s^{-1} and data was analysed with a custom built software using Interactive Data Language (ITT Visual Information Solutions, Boulder, CO, USA). Hearts were stained with a voltage sensitive dye, di-4 ANEPPS (Invitrogen, Carlsbad, CA, USA), using 25 μl of stock solution (1 mg ml^{-1} of dimethyl sulfoxide, DMSO) delivered through a bubble trap, above the aortic cannula. ECG and perfusion pressure were continuously monitored (Powerlab, ADInstruments, Colorado Springs, CO, USA). Hearts were monitored for adequate perfusion throughout the study by visual inspection for pink hue, homogeneous fluorescence and action potential shape (with prominent plateau phase). Typically, data sampling was begun 10 s post-change in pacing CL and was completed within 30 s of rate change (see protocol below).

Stimulation protocol

All hearts were initially challenged with our standard protocol (Banville & Gray, 2002; Hayashi *et al.* 2007; Brunner *et al.* 2008) of decrement in pacing CL consisting of 10 ms steps with progressively shorter cycle length (CL) until loss of 1 : 1 capture or VF induction. Shortening of CLs induced alternans in both LMC and LQT2 (see Fig. 1*B*). While this standard protocol consistently generated DA in the LQT2 rabbits, it usually failed to generate DA in LMC rabbits. Only 1 of 5 LMC hearts demonstrated DA with this standard protocol, in contrast to 5 of 5 LQT2 hearts ($P = 0.024$ compared to LMCs). Since we were interested in comparing the mechanism by which DA can occur in the arrhythmia prone LQT2 hearts and normal controls, we further refined our stimulation steps (~2–5 ms instead of 10 ms) to increase DA induction in LMC hearts as previously done in the rabbit heart (Hayashi *et al.* 2007). With this more gradual decrement in pacing CL, 3 of the 4 remaining LMCs demonstrated DA. Thus, combining both protocols a total of four LMC and five LQT2 hearts demonstrated DA. These nine hearts were used in analyses comparing mechanisms of DA.

Data analysis

The activation and repolarization time points at each site were determined from fluorescence (F) signals by calculating $(dF/dt)_{max}$ and $(d^2F/dt^2)_{max}$, which has been shown to coincide with ~97% repolarization to baseline and recovery from refractoriness (Efimov *et al.* 1994). Data were filtered using a spatial Gaussian filter (3 × 3 pixel) and first/second derivatives (dF/dt, d^2F/dt^2) were calculated using polynomial filter (3rd order, 13 points). Pixels with low signal-to-noise ratio determined by $(dF/dt)_{max}$ (lower than 3 × σ of baseline) and outliers of pixels determined by Grubbs's test were removed from the analysis (typically less than 1% of total pixels). APD dispersion was defined as APD|max – min| across the field of view.

Figure 1*B* shows sample traces from LMC and LQT2 rabbits during baseline and APD alternans. Note that the degree of APD oscillation was greater in LQT2 compared to LMC. Furthermore, during alternans, the action potential rise in some traces occurs before full recovery of the previous action potential as shown in Fig. 2*A*. This phenomenon is likely to have been due to spatial and depth summation of the optical signals from a surface area of 150 μm × 150 μm and depth of ~600 μm. In addition,

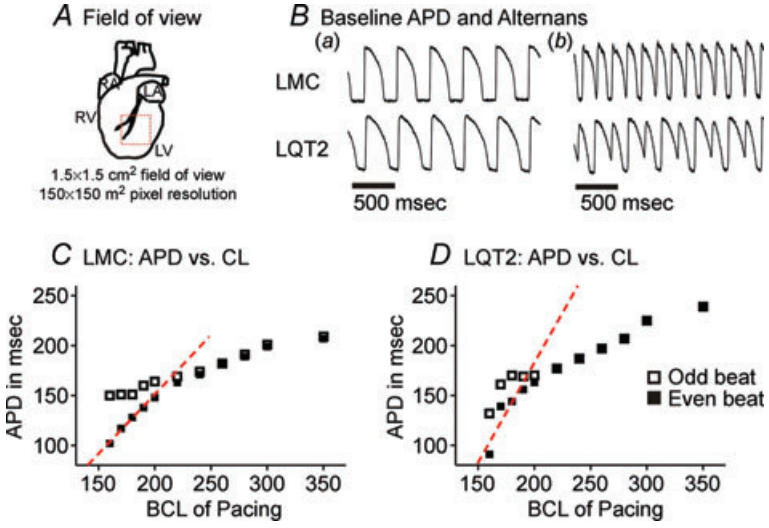

Figure 1. Action potential recordings and APD restitution
A, typical heart field of view (1.5 cm × 1.5 cm, red square) is represented by the cartoon with the position of left anterior descending artery. *B*, sample fluorescence recording. *a*, APD at 350 ms CL in LQT2 was substantially longer than LMC (see text for further detail). *b*, the decrease of CLs triggered APD alternans in both LMC and LQT2 (CL = 160 for LMC and 190 for LQT2 in the examples provided). *C* and *D*, APD restitution in LMC and LQT2, respectively. APDs were averaged from all pixels in the field of view and plotted against CLs. At short CLs, APDs alternate between long (□) and short (■). The slope of APD restitution was measured from even beats with short APDs.

© 2009 The Authors. Journal compilation © 2009 The Physiological Society

light scattering and the spatial filter used (see above) may cause further signal summation (Bray & Wikswo, 2003; Mironov *et al.* 2006; Pertsov *et al.* 2006; Bishop *et al.* 2007*a*,*b*). In such a case, $(d^2F/dt^2)_{max}$ cannot be used to reliably detect repolarization time points, and instead 75% recovery time was used to measure repolarization and repolarization dynamics. The diastolic interval using 75% APD recovery can be overestimated at high CLs, thus affecting APD restitution plots. To avoid this issue, we generated plots of APD restitution by plotting APD as a function of activation interval (AI) at the site of recording, rather than diastolic interval (DI). During alternans, two y values exist for each x value at the same pacing CL. We defined the slope of APD restitution as the slope of the linear regression line generated using the shorter APD during alternans at the four shortest pacing CLs achieved (Fig. 1*C* and *D*). APD restitution dispersion was defined as |max – min| of this slope across the field of view. Although this slope is not the correct restitution slope, the slope of APD restitution as defined here is sufficient to represent spatial dispersion trends and heterogeneous APD restitution in the heart. Note that in Fig. 1*D*, LQT2 exhibits APD shortening in both even and odd beats during alternans. This is due to the occurrence of DA (see details in Result), where long and short APD across the field of view occur in both even and odd beats and are averaged together.

Local conduction velocity (CV) vectors were calculated for each pixel from the differences in activation time-points of that pixel (determined from $(dF/dt)_{max}$) and its 7×7 nearest neighbours, as previously described (Efimov *et al.* 1994). Local conduction velocities were averaged and represented as means ± standard deviation. Local CV can be overestimated when two wave fronts collide, transmural conduction occurs, or near the stimulation site where a small area of tissue was stimulated simultaneously. To correct this error, CVs greater than $1.0\ m\ s^{-1}$ were removed from mean/standard deviation statistics. CV restitution as a function of pacing CL was also analysed. Nodal lines were detected automatically. This algorithm was previously used to construct nodal lines in computer modelling studies (Echebarria & Karma, 2007) and our high signal to noise ratio (100 : 1) allows us to apply the same algorithm to detect small changes in APD during alternans correctly (see Results for details). The norm vector of each pixel on a nodal line was calculated and compared with the CV vector obtained from the activation map by generating the angle of incidence between the two vectors (Jammalamadaka & SenGupta, 2001).

Statistical analysis

Normally distributed continuous variables were compared using Student's unpaired t test. Angle of incidence between vectors in LMC and LQT2 rabbits was compared using a Mann–Whitney test. Categorical values were compared using a Fisher's exact test. Statistical significance was set at $P < 0.05$. Mean data in the manuscript are represented as ±S.D.

Results

Induction and detection of discordant alternans in LMC and LQT2

We previously reported that dispersion of APD in LQT2 rabbits is an important factor underlying arrhythmogenesis (Brunner *et al.* 2008). Here we further examined rate-dependent dynamics of APD dispersion and their relationship with long QT related arrhythmias. Nodal lines were automatically detected by locating positions in the field of view that do not demonstrate beat to beat change during alternans (Fig. 2*A*). First, APD was measured and oscillations between each beat were automatically detected. An oscillation of greater than 5% of the previous APD was defined as alternans. Pixels where APD increases in the next beat were assigned a value of +1, while those where APD decreases were assigned a value of −1 to translate APD data into phase data. Pixels that did not change beat-to-beat were assigned a value of 0 and considered as pixels of the nodal lines and shown in the contour maps. All nodal lines generated were verified by visual inspection.

We validated this detection algorithm with another independent algorithm in three hearts. In this second method (Fig. 2*B*), we chose one reference pixel with a signal that demonstrated a large amplitude of alternans and compared this pixel with the signals of all other pixels using a cross-correlation to calculate the phase shift between two signals. When two pixels exhibited discordant alternans, the phase shift required to maximize the cross-correlation would be exactly one pacing cycle length apart. Nodal lines can be drawn between regions that differ in phase. Both algorithms were used initially with data from two LQT2 hearts and one LMC heart. In all three cases, nodal lines generated independently by these two methods were visually nearly identical (see Fig. 2*Ac* and *Bc*). However, the former approach can detect dynamically changing nodal lines with relatively short computation time and was therefore used in all further analyses.

Using our nodal line detection method and the standard pacing protocol, only 1 of 5 LMCs demonstrated DA and accompanying this DA, a non-sustained VF episode (<10 s) was induced with further reduction in pacing CL. In contrast, LQT2 rabbits demonstrated DA in 5 of 5 hearts. In four of these LQT2 hearts, sustained VF was also induced with further reduction of pacing CL ($P = 0.04$ compared to LMCs). In one LQT2 heart, non-sustained

© 2009 The Authors. Journal compilation © 2009 The Physiological Society

VF was induced only. This disparity in VF induction with 10 ms progressive decrement in pacing CL is similar to results previously described (Brunner *et al.* 2008). With the second pacing protocol, an additional 3 of 4 LMC hearts demonstrated DA. In two of these LMCs, DA was associated with induction of sustained VF.

As an initial survey of alternans behaviour in our two groups, we investigated the pacing CL at which concordant and discordant alternans occurred. A propensity for earlier onset of concordant APD alternans was seen in LQT2 compared to LMCs, though this trend was not statistically significant (236 ± 22 ms *vs.* 208 ± 23 ms, respectively; $P = 0.08$). In contrast, a significant difference was seen in DA onset. The mean pacing CL at which DA was detected in LQT2 was 206 ± 24 ms, which corresponds to a heart rate of 291 bpm. This heart rate is within the physiological range for rabbits. In LMC, the mean pacing CL at which DA was detected was 156 ± 5 ms ($P = 0.011$

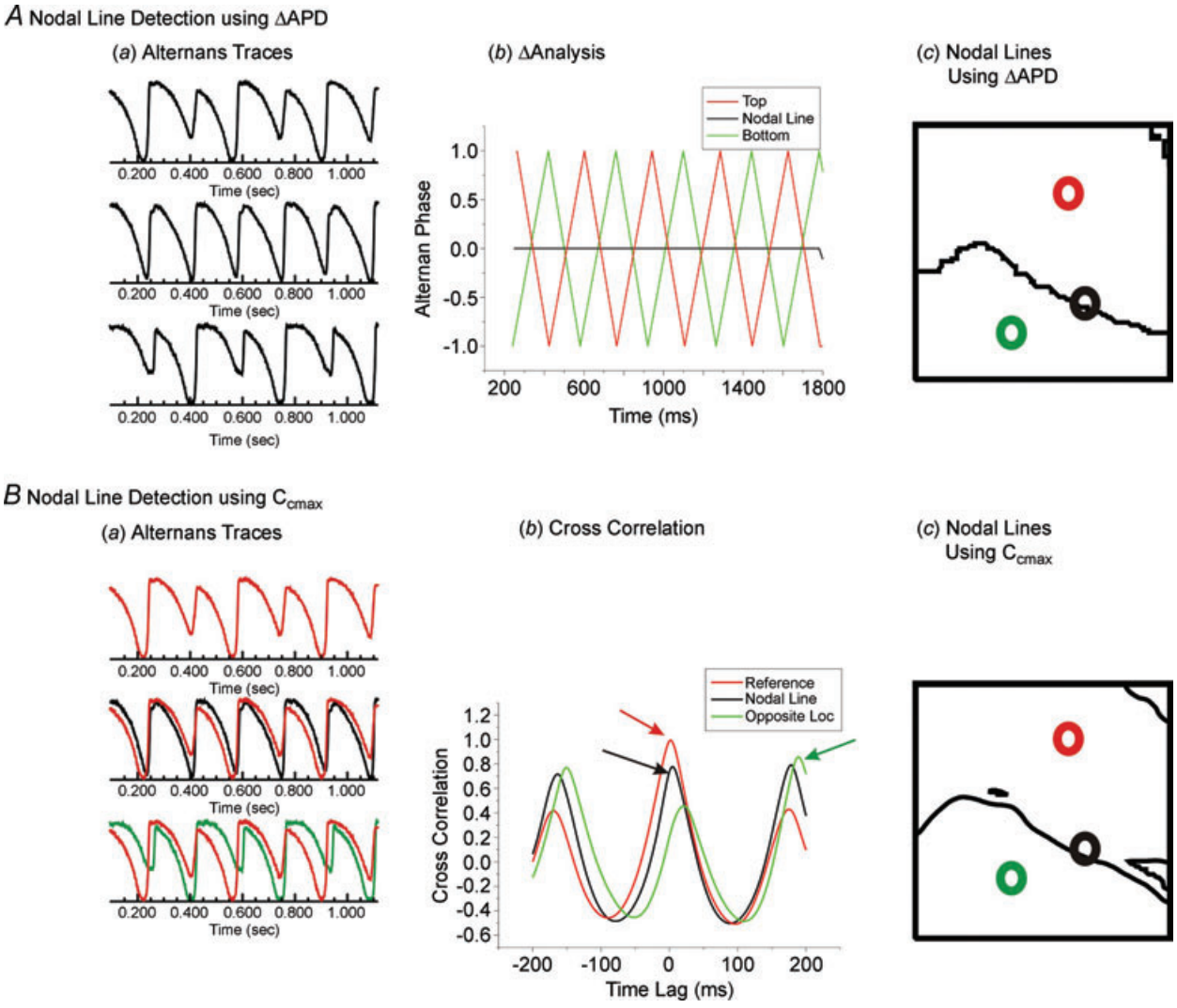

Figure 2. Nodal line detection
A, nodal line detection using ΔAPD. *a*, APD alternans in an LQT2 heart. *b*, phase of alternans at each pixel was represented as +1 when the following APD is longer, −1 when the following APD is shorter, and zero when ΔAPD is within small variation (<5%) (black line). *c*, after filtering alternans phase maps with a 15 × 15 Gaussian filter, contour lines were drawn along the zero phase (black) to divide two regions alternating out of phase (red and green). *B*, nodal line detection using cross-correlation. *a*, signal from reference location (red) at top trace, overlapped with a trace from a nodal line region (black) and out-of-phase region (green). *b*, cross-correlation will give the maximum correlation when a time delay between two signals is introduced such that their overlap is optimized. When discordant alternans occurs, two locations that are out of phase will have maximum correlation at the delay of one cycle length, signifying APD oscillation is out of phase (see green lines in the trace and cross-correlation plots). When a region with APD alternans is cross-correlated with a nodal line region, maximum correlation remains constant at delay the one cycle length (black). *c*, contour lines are drawn separating out of phase regions. Both methods showed compatible patterns of nodal lines.

© 2009 The Authors. Journal compilation © 2009 The Physiological Society

for LMC *vs.* LQT2 DA CL onset), corresponding to a heart rate of 385 bpm. Furthermore, the difference in onset of concordant and discordant alternans was significantly smaller in LQT2s compared to LMCs (22 ± 13 ms *vs.* 55 ± 24 ms respectively; $P = 0.03$). Of note, in our experience, sinus rates of free moving rabbits do not exceed 300 bpm (Nishida *et al.* 2002; Brunner *et al.* 2008). Therefore, we believe that DA induced *ex vivo* in LMCs is likely to be a non-physiological phenomenon, while DA induced in LQT2 rabbits may play a role in this model's propensity for spontaneous ventricular arrhythmias.

Discordant alternans in LMC and LQT2 and relation to conduction velocity

We analysed the behaviour of DA nodal lines at the onset of DA (as detected by our algorithm) in the nine hearts that demonstrated DA (LMC = 4 and LQT2 = 5). Figure 3 shows typical examples of activation and repolarization maps from odd and even beats, and sample traces demonstrating DA. Figure 3*A* shows data from a LMC heart. Sample traces on the left column demonstrate out-of-phase alternans. Between these out-of-phase regions, a nodal line exists where the APD does not oscillate beat-to-beat and is shown as a red line on the repolarization maps. Figure 3*B* shows maps and sample traces recorded from LQT2 rabbits. Note that the nodal line in the LMC is relatively aligned with activation wave fronts. Theoretically, if CV restitution drives the onset of DA, then DA would form between a region near the pacing site and a region far from the pacing site. Furthermore, we postulated that if CV restitution drives the onset of DA, the two regions of DA would be separated by slow conduction and therefore DA nodal lines would align with activation isochronal lines. This is the behaviour demonstrated by all four LMCs with DA in line with earlier studies by other groups (Hayashi *et al.* 2007; Mironov *et al.* 2008), suggesting CV restitution in this control group is a major factor in generating DA. This result is also consistent with DA occurrence in LMCs using the second protocol, with a smaller decrement in CL. To cause significant CV slowing and beat-to-beat CV alternans, one must pace near relative refractoriness. Thus, it is only when we near relative refractoriness in LMCs that DA occurs in this group.

In contrast, the nodal line in the LQT2 (Fig. 3*B*) does not appear congruent with the activation wave front. The nodal line transects through activation isochronallines, suggesting that DA is occurring between two regions with no relative activation delay. This type of nodal line formation is not consistent with CV restitution as an underlying mechanism for DA onset. This was the pattern seen in 4 of the 5 LQT2s at the onset of DA ($P = 0.04$).

To further quantify concordance between activation wavefronts and nodal line formation in our two groups, we compared the angle of incidence of the activation vector and the nodal line norm vector as described in detail in Methods. A greater concordance in activation and nodal line vectors was seen in LMC compared to LQT2, with an angle of incidence of 32 ± 3 deg compared to 46 ± 3 deg, respectively ($P = 0.034$). Thus, LQT2 rabbits demonstrate significantly different characteristics of nodal lines during DA.

Modelling studies (Qu *et al.* 2000) predict that with DA resulting from oscillations in conduction velocity nodal lines will form distal to the pacing site and therefore a change in pacing site would yield a major shift in nodal line position. We tested this hypothesis in LMC and LQT2 hearts with pacing from several locations ($n = 2$ for each group). Figure 4*A* demonstrates how changing pacing sites influences the location of nodal lines. In the LMC heart, a change in pacing site is accompanied by a complete shift in the nodal line formed to accommodate the activation wavefront. With both pacing sites, nodal lines in the LMC remain well correlated to activation isochronal lines. However, in LQT2, a change in pacing site only has a partial effect. The nodal line appears to retain its basic shape and location despite the change. This resistance to the change in activation wavefront underscores the relative independence of DA to activation interval and CV changes and suggests that CV restitution is not a major contributor to LQT2 nodal line formation at this longer pacing CL when DA onset is seen.

Next, we examined the onset of DA and its relationship to CV restitution to pacing CL, since the conduction velocity restitution hypothesis requires that beat-to-beat oscillation in CV occur prior to onset of DA. Figure 4*B* shows plots of mean CV and APD dispersion as a function of pacing CL. Since the immediate effect of DA onset is the increase in APD dispersion, here we tracked APD dispersion as a function of pacing CL as a verification of onset of discordant alternans. Arrows in Fig. 4*B* represent DA incidence by our nodal line detection in LMC (red) and LQT2 (black). Onset of DA occurred at longer pacing CL in LQT2 compared to LMC, consistent with the requirement that relative refractoriness of the tissue for slow conduction be reached for onset of DA in LMC, but not in LQT2. Mean onset of DA in LMC is coincident with a doubling of APD dispersion and occurs only after a greater than 10% decrement in CV from baseline. In LQT2, mean onset of DA was also coincident with a doubling of APD dispersion. However, DA onset precedes any significant reduction in mean CV. Furthermore, with DA initiation in LQT2, mean CV was significantly greater than mean CV in LMC at DA onset (0.66 ± 0.09 m s^{-1} *vs.* 0.47 ± 0.12 m s^{-1}; $P < 0.05$), supporting the concept that DA in LQT2 does not require decrement in CV.

© 2009 The Authors. Journal compilation © 2009 The Physiological Society

To further illustrate the differential contribution of CV to DA in LMCs and LQT2s at the onset of detectable DA, we generated simultaneous plots of CV, activation interval (AI), diastolic interval and APD across a distance in the field of view spanning from the stimulation site through the region of DA represented by the dashed red line shown in Fig. 4*C* on the activation and the repolarization maps. Plots of CV, AI, DI and APD across the nodal lines are shown. Hearts were stimulated from the right side of field of view (left ventricle free wall) marked by the green square wave and activation waves propagate from the right to left. In the graphs, the pacing site is represented at the far right of the *x* axis at 0 mm. Our experimental results deviate from the exact outcome from computer modelling predictions in the behaviour of AI oscillations, where an expected AI maximum oscillation occurs at the APD nodal line. However, as predicted by the CV restitution hypothesis, CV plots in the LMC exhibit the oscillation

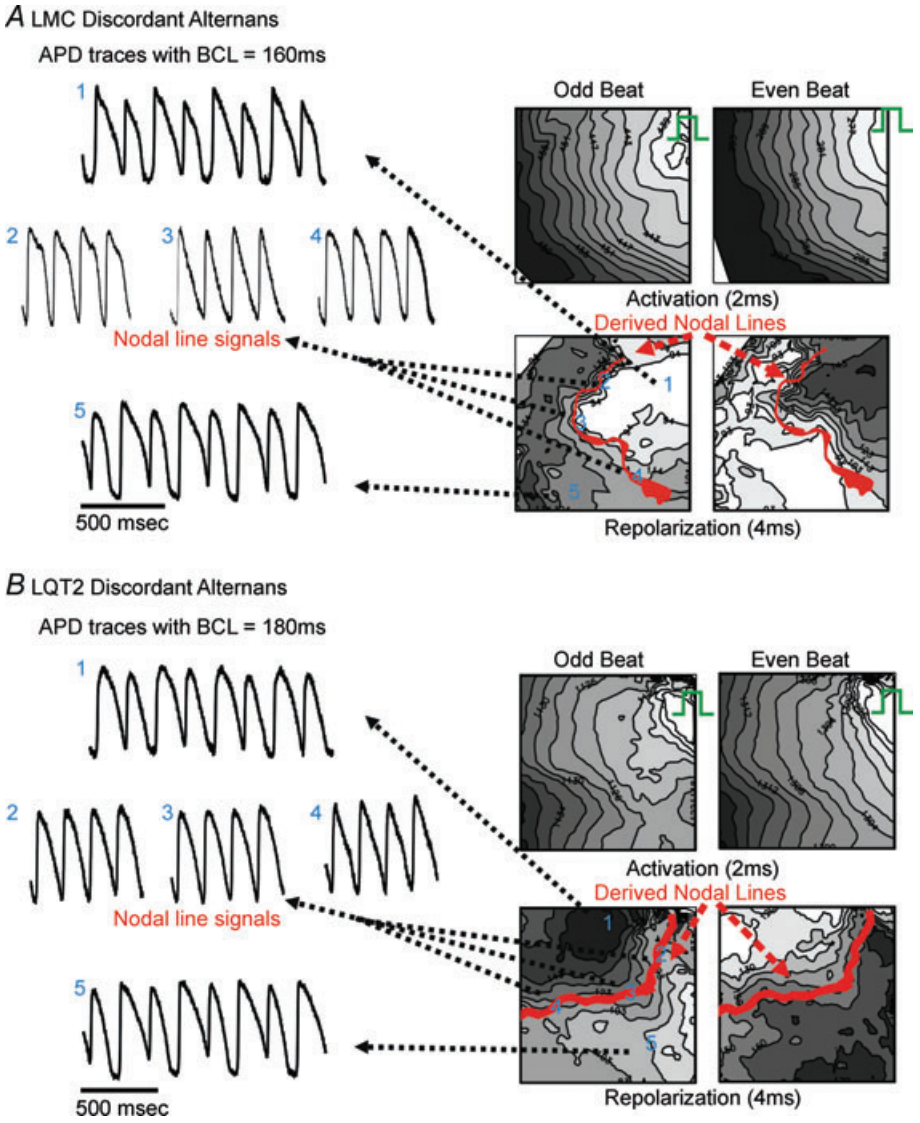

Figure 3. Discordant alternans in LMC and LQT2 hearts
A, activation and repolarization maps during DA in a LMC paced at CL of 160 ms. Sample traces are shown in left panels from regions (labelled 1–5) in the repolarization maps. Top maps demonstrate activation (2 ms isochronal lines) with stimulation from the right upper corner of the maps (green square wave) and wavefront propagation from light to dark. Bottom maps demonstrate repolarization maps (10 ms isochronal lines) with out of phase (discordant) repolarization alternans in regions near and far from the pacing site. A nodal line forms between these two regions that is congruent with activation isochronal lines, consistent with CV restitution hypothesis of DA mechanism. Sample raw traces of optical signals from the nodal line (numbered 2–4) and from either side of the nodal line are shown on the left of maps. *B*, activation and repolarization maps during DA in LQT2 paced at CL of 180 ms. A nodal line forms (traces 2–4) between two regions that is incongruent with activation isochronal lines, contrary to the CV restitution hypothesis of DA mechanism.

© 2009 The Authors. Journal compilation © 2009 The Physiological Society

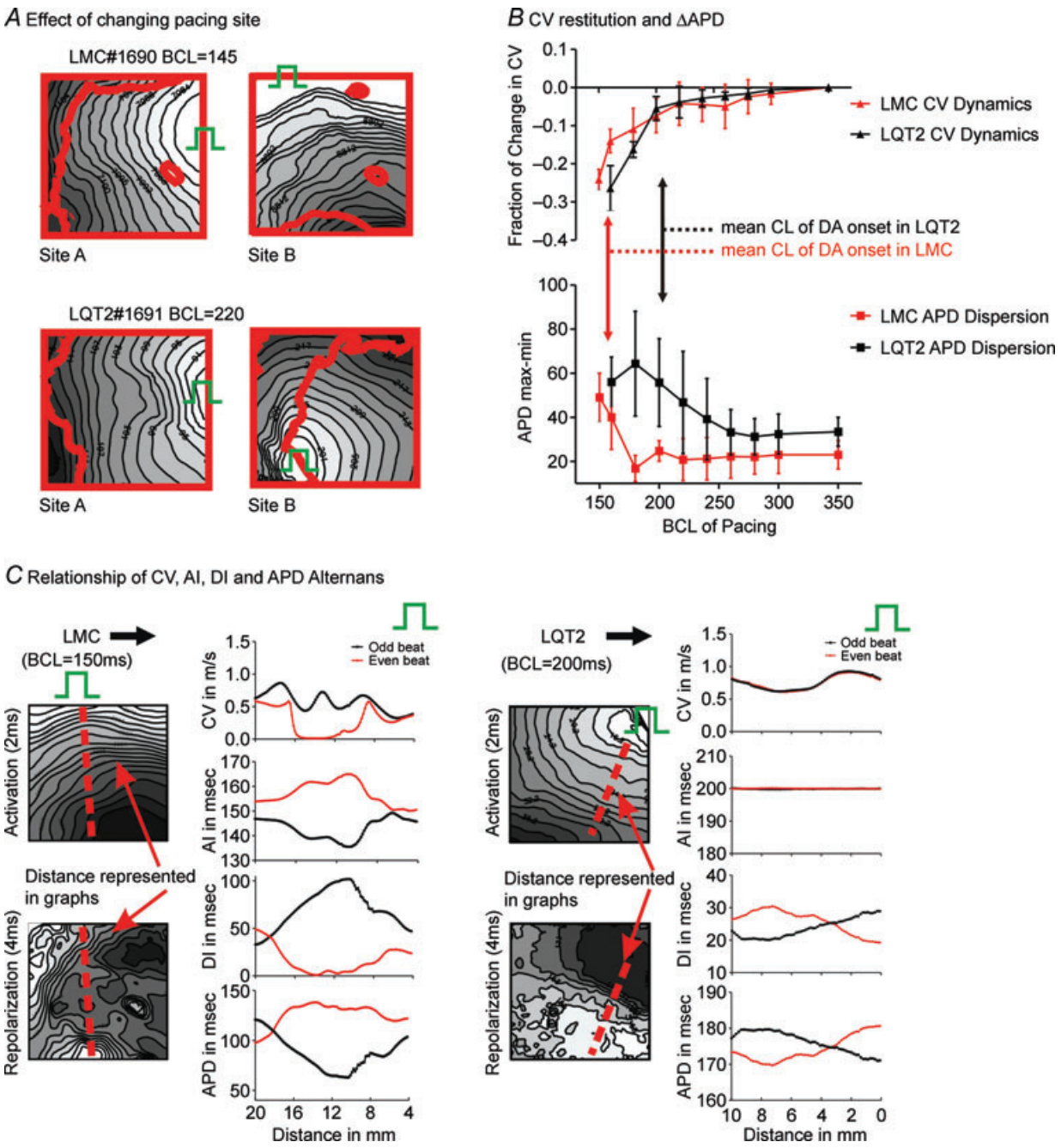

Figure 4. Relationship of CV restitution to the onset of discordant alternans
A. Effect of changing pacing site. Note that nodal line pattern changes after moving the pacing site in LMC while nodal lines were relatively stable regardless of pacing site in LQT2. *B*, CL-dependent changes in CV and APD dispersion. Fractional change in CV is plotted against pacing CL with notable slowing at CLs shorter than 200 ms in both LMC and LQT2. The mean onset of detected DA in LMCs (red) and LQT2s (black) is marked by the arrows. Note that with occurrence of DA, ΔAPD increases in both genotypes, mean DA of LQT2 occurring at 206 ms pacing CL and of LMCs occurring at 156 ms pacing CL. A significant fractional reduction in CV is seen prior to DA onset in LMCs, but not in LQT2s. *C*, CV, AI, DI, and APD plotted across a single distance spanning from the stimulation site through an out-of-phase region in LMC and LQT2 hearts. Activation and repolarization maps are shown on the left columns and the graphs of CV, activation interval (AI), diastolic interval (DI) and APD over the red dashed lines on the maps are shown on the right columns. Odd and even beats are represented on each graph as black and red curves, respectively, and activation proceeds from pacing site (green square wave) on the right toward the left. LMC (left) graphs demonstrate beat-to-beat CV alternans 10 mm closer to the pacing site than the APD nodal line; consistent with CV restitution driven APD discordant alternans. In contrast, LQT2 (right) graphs demonstrate no significant CV or AI beat-to-beat alternans yet a large out-of-phase DI and APD alternans were seen, suggesting DA can occur without CV alternans in the LQT2 case.

© 2009 The Authors. Journal compilation © 2009 The Physiological Society

between even and odd beats with maximum reduction coincident with APD maximum oscillations. Consistent with CV oscillations, AI plots in the LMC also demonstrate oscillation between even and odd beats. Furthermore, CV beat-to-beat alternation precedes changes in beat-to-beat alternation in DI and APD along the represented distance, suggesting that alternating CV between odd and even beats creates heterogeneous AI changes that produce discordant alternans. In contrast to the LMC case, DA in LQT2 hearts occurred without the accompanying beat-to-beat changes in CV or AI, as demonstrated in Fig. 4*C* (far right graphs). This finding is consistent with no apparent reduction in CV in LQT2 hearts at the time of onset of DA and furthermore highlights the relative independence of DA onset in LQT2 from CV alternans compared to LMCs. All four LMCs demonstrated CV alternans more proximal to the stimulation site compared to the nodal line of DA, which occurred more distally from the stimulation site using this analysis described above. None of the five LQT2s demonstrated this relationship of CV alternans more proximal to the nodal line of DA ($P = 0.008$). Of note, CV along the lines drawn in both genotypes is not constant but shows a sinusoidal-like pattern. This is most likely to be due to the fact that CV changes are dependent on the anisotropic conduction along the muscle fibres. Nonetheless, beat-to-beat oscillations in CV and AI plots only occurred in LMCs and clearly demonstrate that DA in our LMC hearts is due to CV restitution, compatible with earlier studies (Watanabe *et al.* 2001; Hayashi *et al.* 2007).

Spatial heterogeneity and discordant alternans in LMC and LQT2

Theoretical studies have demonstrated that if sufficient spatial heterogeneity in repolarization exists, DA can occur with shortening of pacing CL or premature stimuli (Watanabe *et al.* 2001). Therefore, we examined the extent of repolarization heterogeneity in the LQT2 hearts compared to LMCs. We investigated baseline heterogeneity as represented by APD dispersion at a pacing CL of 350 ms and heterogeneity in APD restitution (as described in Methods).

Mean APD in LQT2 was significantly longer than LMC (251 ± 17 ms *vs.* 217 ± 8 ms; $P = 0.007$). As seen in our previous investigation (Brunner *et al.* 2008) APD dispersion was also significantly increased in LQT2. Figure 5*A* demonstrates APD maps from two

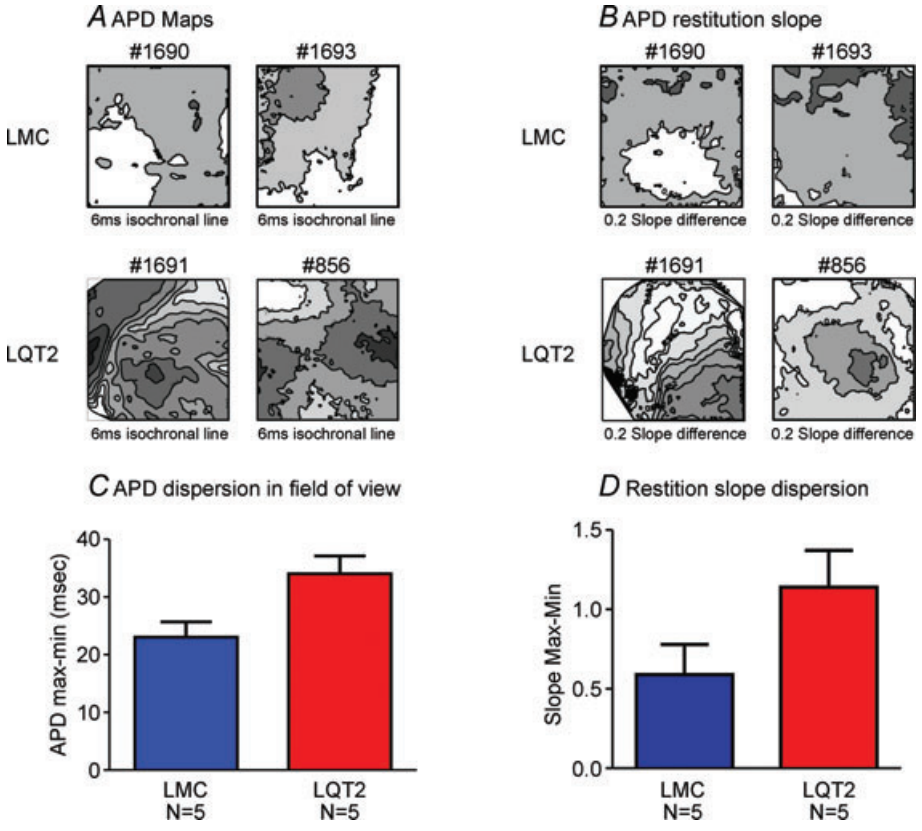

Figure 5. Repolarization heterogeneity in LMC and LQT2 hearts
A, examples of APD maps at 350 ms BCL. *B*, examples of APD restitution slope maps. *C*, APD dispersion in LMC and LQT2. *D*, APD restitution slope dispersion in LMC and LQT2. Note that LQT2 shows higher APD dispersion and APD slope dispersion.

© 2009 The Authors. Journal compilation © 2009 The Physiological Society

representative LMC and LQT2 hearts, with demonstration of greater APD dispersion in LQT2s as displayed by their greater number of isochronal lines (representing a difference of 4 ms). We found a mean $APD_{|max-min|}$ of 34 ± 7 ms in LQT2s compared to an $APD_{|max-min|}$ of 23 ± 6 ms in LMCs ($P = 0.03$) (Fig. 5*C*). Similar to our findings in baseline comparisons of APD, APD restitution was significantly different in LMCs and LQT2s. The mean APD restitution slope demonstrated a trend toward steeper slope in LQT2s compared to LMCs with slopes of 0.83 ± 0.13 and 0.64 ± 0.11, respectively ($P = 0.056$). Figure 5*B* demonstrates APD restitution slope maps from two representative LMC and LQT2 hearts. These maps show greater slope heterogeneity in LQT2s as displayed by their greater number of isocontour lines (representing a difference of 0.2 slope) in the maps. While the limitations of optical signals (see Methods) may alter absolute measurements of APD and its restitution, a qualitative comparison demonstrates a significant difference in the dispersion of APD restitution between LMCs and LQT2s as measured by the mean $slope_{|max-min|}$ of APD restitution. The mean slope dispersion was 1.14 ± 0.22 in LQT2s and 0.56 ± 0.19 in LMCs ($P = 0.001$) (Fig. 5*D*).

We further examined the correlation between the onset of DA and measurements of heterogeneity. Figure 6*A* shows plots of APD dispersion *versus* pacing CL at onset of DA in LMC and LQT2 rabbits. We found a statistically significant correlation between APD dispersion and onset of DA in LQT2 hearts but not in LMCs ($r = 0.20$ in LMC, NS for slope different than 0; $r = 0.95$ in LQT2, $P = 0.014$ for slope different than 0). According to previous computer modelling studies of DA (Qu *et al.* 2000; Watanabe *et al.* 2001; Echebarria & Karma, 2007), the key component to DA formation by tissue heterogeneity is the extent that two regions differ in their dynamic behaviour of APD when stressed with a premature beat or shortening of pacing CL. Therefore, we subsequently investigated the relationship of the dispersion in APD restitution to DA onset CL (Fig. 6*B*). In LMCs, no correlation was observed between these two variables ($r = -0.17$, NS for slope different than 0). However, LQT2 rabbits exhibited a strong correlation between slope dispersion and DA onset CL ($r = 0.98$, $P = 0.003$ for slope different than 0). This trend suggests an important influence of spatial heterogeneity in APD restitution on the onset of DA in LQT2. Interestingly, dispersion of APD restitution demonstrated a stronger correlation to CL at onset of DA compared to baseline dispersion in APD. These results are consistent with the fact that dispersion of APD restitution is closely linked to DA generation due to tissue heterogeneity.

We further reasoned that if spatial heterogeneity in APD and its restitution were critical to onset of DA in LQT2 hearts, a detectable difference in the restitution gradient would be discernable between regions that support a nodal line and those that do not. Figure 6*C* illustrates an example of DA and nodal line formation (repolarization maps, right) and its relationship to spatial heterogeneities in APD restitution slope (slope map, left). Nodal lines conform to regions where slope isocontour lines appear crowded. To quantitatively assess this relationship of nodal line location and APD dispersion, we calculated the local APD and APD restitution slope gradients at nodal line locations and the remainder of the field of view. In LMCs, APD gradient at nodal lines did not differ significantly from the surrounding regions in the field of view (1.5 ± 0.7 ms mm^{-1} *vs.* 1.2 ± 0.8 ms mm^{-1} respectively; NS), while in LQT2 hearts mean APD gradient at nodal line regions was significantly increased compared to surrounding regions (2.4 ± 0.5 ms mm^{-1} *vs.* 1.9 ± 0.5 ms mm^{-1} respectively; $P = 0.03$). Gradient in restitution slope demonstrated a similar trend with no significant difference seen between regions of nodal lines and surrounding areas (0.11 ± 0.1 mm^{-1} *vs.* 0.1 ± 0.8 mm^{-1} respectively; NS). However, in LQT2 hearts again a strong regional relationship emerges between slope gradient and nodal line location (0.16 ± 0.02 mm^{-1} *vs.* 0.1 ± 0.003 mm^{-1} respectively; $P = 0.003$). Thus, as predicted by the tissue heterogeneity hypothesis, we find a spatial correlation between nodal lines and steep gradients in APD and its restitution in LQT2 hearts.

Unstable nodal lines in LQT2 hearts

While tissue heterogeneity appears well correlated with initial onset of DA in LQT2 and CV beat-to-beat alternans is absent at the initial detection of LQT2 DA, these relationships became more complex as pacing CL was progressively shortened in the LQT2 hearts (see Fig. 7*A*). Activation (top) and repolarization (bottom) maps for odd and even beat are shown at a pacing CL of 190 ms when DA was initially detected (left panels) in an LQT2 heart. As seen previously the nodal lines appear incongruent with activation isochronal lines, and thus likely are being formed by tissue heterogeneity across the field of view. However, as the pacing CL is shortened to 170 ms (Fig. 7*A*, right panels), a new nodal line also emerges parallel with the activation wave front and associated with slowing of CV as demonstrated by the closely spaced isochronal lines in the odd beat activation map (red asterisk). This new nodal line at a shorter pacing CL in this LQT2 heart is now consistent with CV restitution driven DA. This behaviour was seen in the two LQT2 hearts where pacing at a CL less than or equal to 170 ms was possible prior to VF induction. (The 3 other LQT2 hearts all had VF at 180 ms pacing CL or greater.) Thus as LQT2 hearts were exposed to the pacing CLs that were required for LMC DA onset,

© 2009 The Authors. Journal compilation © 2009 The Physiological Society

CV restitution appeared to influence nodal line behaviour in LQT2s as well.

To further understand nodal line behaviour when two potential drivers of DA co-exist in the same heart as in LQT2s when successfully paced at <170 ms CL, we overlapped 50 consecutive beats of DA at pacing CLs of less than 170 ms in both LMCs and LQT2 hearts and analysed the relationship of nodal lines to contour maps of activation, baseline APD and APD restitution. Figure 7*B* represents overlapped nodal lines from 50 consecutive beats in a LMC and LQT2. The LMC overlapped nodal lines appear as a relatively uniform band, suggesting that nodal lines from multiple beats appear very stable in the LMC (left panel). In contrast, LQT2 overlapped nodal lines appear disorganized and expansive, suggesting that within these 50 consecutive beats, nodal lines are unstable with beat-to-beat changes in LQT2 (right panel). Figure 8*A* demonstrates this beat-to-beat alteration in nodal line behaviour. Beats 18 through 23 from a set of 50 consecutive APD phase maps are shown from an LQT2 rabbit with pacing at a 160 ms CL. Within these six beats, three distinct phase map patterns are seen. A shift of phase map appearance occurs between beats 18 and 19 (pattern A to pattern B). Subsequently instability and shifting in

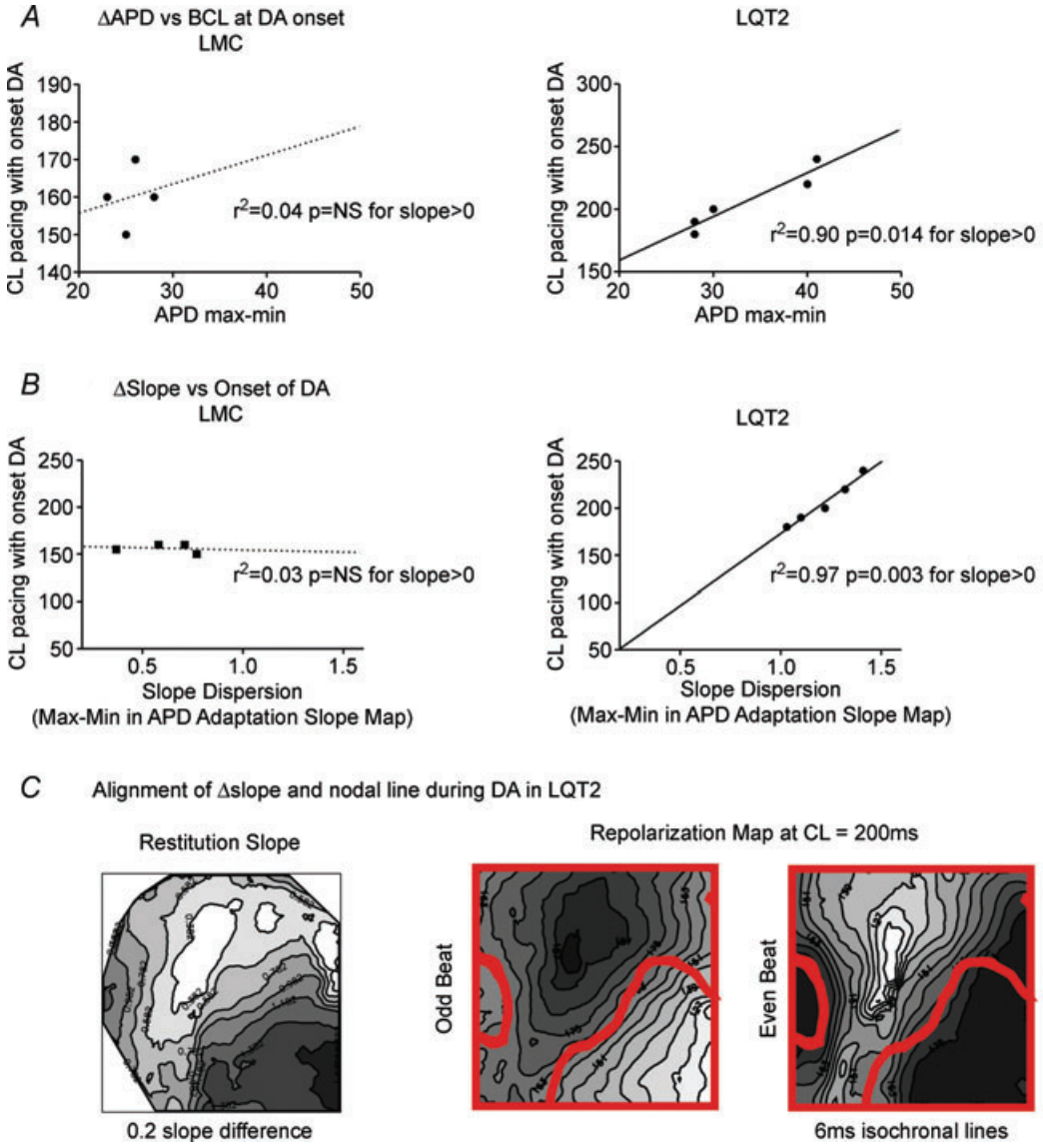

Figure 6. Correlation between the onset of DA and repolarization heterogeneity
A, the onset of DA plotted as a function of APD dispersion in LMCs (left) and LQT2s (right). *B*, the onset of DA plotted as a function of APD restitution slope dispersion in LMCs (left) and LQT2s (right). LMCs do not show statistically significant correlation between DA onset and both measures of repolarization heterogeneity, suggesting that higher APD dispersion is responsible for DA at longer CLs. *C*, Nodal lines show best alignment with regions of highest gradient of restitution slope (closest isocontours) in LQT2.

© 2009 The Authors. Journal compilation © 2009 The Physiological Society

the discordant regions is seen in the following four beats, with the APD phase maps shifting to pattern C and subsequently back to pattern B (beat 23). Recording of signals during this rapid pacing from map positions 1–4 are shown in Fig. 8*B*. Positions 3 and 4 in the maps above demonstrate the greatest nodal line shifts and traces from these positions demonstrate multiple phase shifts in APD alternans during these six beats. These recordings took place between 10 and 30 s after the change in pacing CL (typically from 170 ms to 160 ms). Therefore, the persistence of shifting nodal lines in this model cannot be explained by short term cardiac memory.

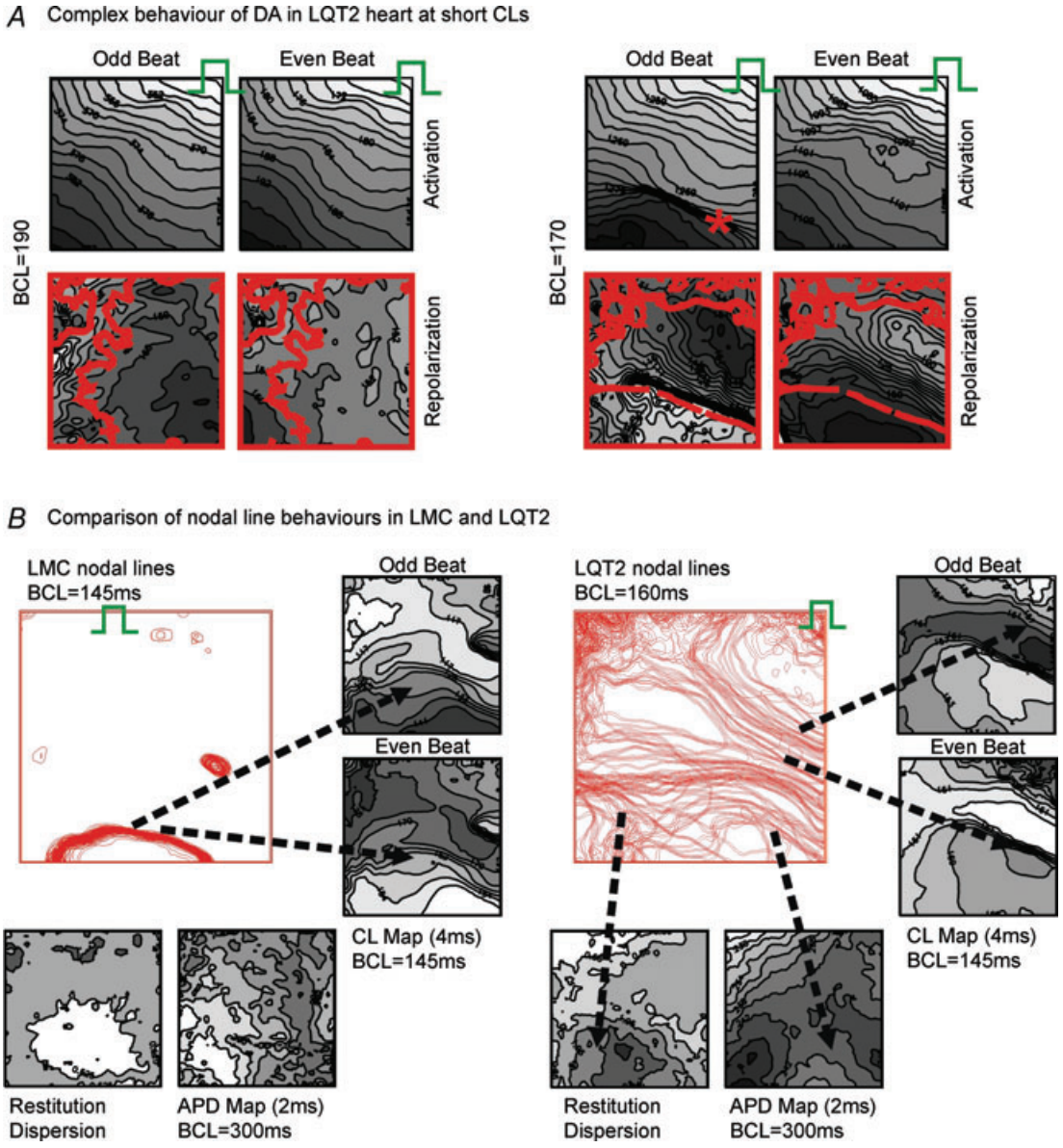

Figure 7. Competing influence of tissue heterogeneity and CV restitution on spatially discordant alternans

A, complex nodal line behaviour in LQT2. Nodal lines at different CLs were superimposed on activation and repolarization maps of odd and even beats. At slower pacing CL, nodal line formation is correlated poorly to activation wave fronts. However, with a shorter pacing CL, a new nodal line also forms congruent with activation isochronal lines, demonstrating contribution from both CV restitution and tissue heterogeneity in this LQT2 at the shorter pacing CL. *B*, example of superimposed nodal lines from 50 consecutive beats in a LMC (left) and LQT2 (right) heart (pacing site marked by green square wave) at a short CL pacing. Restitution slope maps and APD maps for each heart are shown below. To the left of the nodal lines, odd and even beat cycle length (activation interval) maps are shown during the same pacing sequence. LMC nodal lines conform to cycle length map isochronal lines, but not slope or APD maps. LQT2 nodal lines at this short pacing CL demonstrate contributions from both APD dispersion and CV alternation.

© 2009 The Authors. Journal compilation © 2009 The Physiological Society

We further examined the origin of overlapped nodal lines by directly comparing nodal line maps with activation interval, APD and slope of APD restitution maps. Nodal line alignment with activation interval maps would be consistent with CV restitution driven DA, while alignment with APD or slope maps would suggest repolarization spatial heterogeneity driven DA. In LMCs, APD and restitution maps reveal a poor match with the overlapped nodal lines (Fig. 7*B*, left, bottom panes). However, when compared to maps of the cycle length (activation interval) in odd and even beats (right of LMC nodal lines) a clear correlation is seen between the nodal line position and activation interval map isochronal lines. As expected, in this example of a LMC the 50 overlapped nodal lines draw their shape from changes in cycle length (or AI) and therefore are governed by CV restitution. We applied this same analysis to the more complex nodal line formations in LQT2 (Fig. 7*B*, right panels). At this shorter pacing CL (160 ms), some nodal lines appear to be congruent with the isochronal lines of the beat-to-beat cycle length (activation interval) map, and thus are formed by beat-to-beat AI changes. However, clearly other nodal lines are incongruent with activation. Instead these nodal lines (marked by dashed black arrows) correspond to isocontour lines seen in APD and APD restitution slope maps (below LQT2 nodal line map). This comparison highlights the fact that two competing mechanisms of DA can co-exist in the same heart with each providing a contribution to nodal line formation.

To quantify this comparison, we calculated the percentage of congruency of activation, baseline APD and APD restitution map contours with the contours of the combined 50 beats of nodal lines at pacing CLs of less than or equal to 160 ms. In LMCs, $98 \pm 2\%$ of nodal lines demonstrated congruency with activation (2% indeterminate). Only two LQT2 rabbits were successfully paced at <170 ms prior to VF, both demonstrating complex nodal line behaviour at the short pacing CLs. In these two LQT2 hearts, $70 \pm 1\%$ demonstrated congruency with activation, while $24 \pm 3\%$ demonstrated congruency with APD map isocontour lines (6% indeterminate).These results suggest that at a shorter pacing CL, in the range where CV is decreased (see Fig. 4), both tissue heterogeneity and CV restitution play a role in the formation of nodal lines in LQT2 hearts.

To investigate the contribution of nodal line instability to arrhythmia in LQT2 rabbits, we mapped optical signals just prior to the onset of VF during short CL pacing. Figure 9 depicts such an example. Figure 9*A* shows the restitution slope map of the LV free wall in this LQT2 heart. The heart is paced from a site to the right of the field of view and a DA nodal line forms almost perpendicular to activation wavefront. Traces from above and below the nodal line are shown to the right. APD oscillations appear out of phase above and below the nodal line in beats 3–6 (beats 4–5 are labelled L (long)–S (short)–L (long) accordingly). At beat 7, a delay in activation is seen above the nodal line (labeled Block). Figure 9*B* details the activation, repolarization and nodal line maps of the LV free wall, during beats 4–7 in Fig. 9*A*. DA is

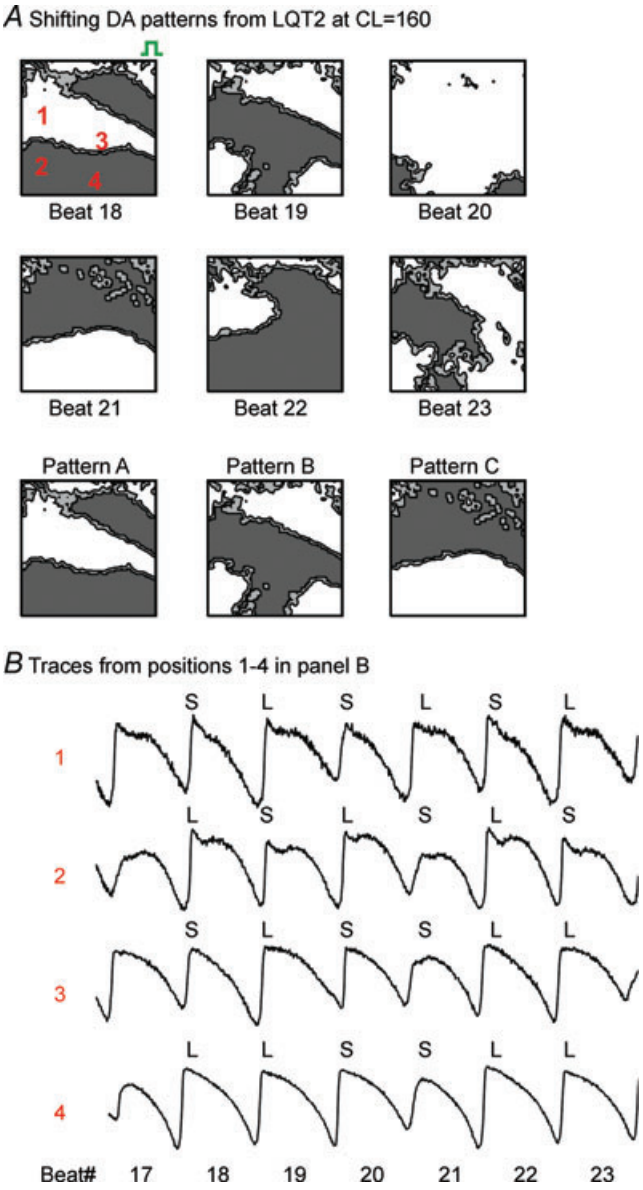

Figure 8. Persistent shifting nodal lines in LQT2 and formation of conduction block
A, phase maps of beats 18–23 of 50 consecutive beats in an LQT2 heart paced at a CL of 160 ms from site marked as a green square wave. Gray and white represent long and short APD alternans phase, respectively. Nodal lines are drawn between gray and white regions. Three distinct patterns of spatially discordant alternans are shown on the right, labelled A, B and C. Large shifts between these 3 patterns are seen over a single beat (see text). *B*, traces are shown from positions 1–4 in phase maps where the largest shifts in phase are seen through beats 18–23. APDs are labelled S (short) and L (long) according to the detection algorithm (see Methods). Positions 3 and 4 demonstrate multiple phase shifts.

© 2009 The Authors. Journal compilation © 2009 The Physiological Society

seen between the base and mid LV free wall parallel to the AV groove and nearly perpendicular to activation isochronal lines, suggesting tissue heterogeneity is likely to be the major contributor to the nodal line formation on these beats. The nodal lines appear to be stable in beats 4–6. In beat 7, a line of conduction block emerges that is congruent with the DA nodal line where a 35 ms delay occurs in the activation of the area of long APD in beat 6 (basal aspect of LV free wall). Activation of this region occurs via epicardial breakthrough on the left (red arrow) and eventually via activation from the right possibly by means of transmural breakthrough (dashed red arrow). The APD and nodal line maps of beat 7 demonstrate a phase shift and synchronization of APD from basal and apical LV free wall. Thus, subsequent to the conduction block, a major shift in nodal line occurs. In Fig. 10, we provide an analysis of CV, AI, APD and DI in the beats preceding the conduction block. First, Fig. 10*A* demonstrates the presence of beat-to-beat oscillation in CV while pacing at 150 ms CL. These oscillations in CV translate to AI oscillations across both sides of the major nodal line (Fig. 10*B* and *C*). The regions above and below the nodal line have different restitution slopes (see Fig. 9*A*) and thus respond differently to small oscillation in AI. While initially (beats 3–4), the region above the nodal line demonstrates smaller APD oscillation compared to the region below the nodal line, an amplification of APD oscillation is seen during beats 5 and 6 in this region (Fig. 10*C*, middle). With this amplification, the APD gradient increases from 56 ms on beat 3 to 83 ms on beat 6. Furthermore DI in this region progressively shortens until a nadir is reached on beat 6 and conduction block occurs, likely to be due to DI reaching the tissue effective refractory period. This example suggests that at rapid pacing of a region with large heterogeneity in restitution, CV oscillations and consequently AI oscillations can amplify dispersion and promote functional conduction block. Conduction block creates regional phase shifts and thus shifting nodal lines. Interestingly this case suggests that while DA onset depends on spatial heterogeneity, in this model, competing CV and tissue heterogeneities in LQT2 and their interaction may play an important role in formation of conduction block and therefore in initiation of reentrant arrhythmias.

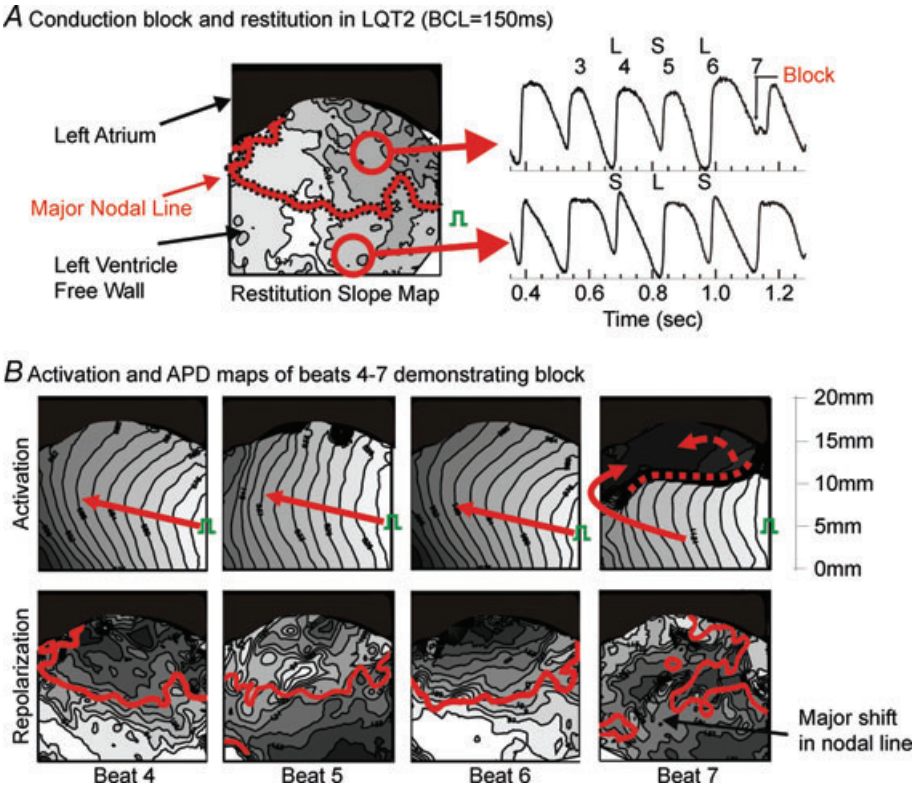

Figure 9. Formation of conduction block and major shifts in nodal lines
An example is shown of an LQT2 heart that was paced at 150 ms CL just prior to the onset of VF. *A*, restitution slope map of the LV free wall with a nodal line formed perpendicular to the activation wavefront (pacing occurs just to the right of the field of view). To the right of the map, traces are shown from above and below the nodal line with discordant APD alternans (S, short; L, long). *B*, activation and repolarization maps of beats 4–7 prior to conduction block. Nodal lines are superimposed on repolarization maps. Note that nodal lines are incongruent with activation patterns initially. Beat 7 demonstrates conduction block at the region above the nodal line where the 'longer' APD on beat 6 occurred.

© 2009 The Authors. Journal compilation © 2009 The Physiological Society

Discussion

Enhanced dispersion and steep restitution have been long suspected as a mechanism underlying long QT related arrhythmias. Here, we used a novel transgenic rabbit model of LQT2 that demonstrates a phenotype of spontaneous ventricular arrhythmias and sudden death (Brunner *et al.* 2008). Our major findings are that (1) dispersion of repolarization in LQT2 is dynamic and is enhanced by discordant alternans (DA); (2) DA was seen even at physiological heart rates in LQT2; (3) in LMCs alternation of CV is responsible for DA, while in LQT2 hearts, heterogeneities in APD restitution play the primary role in DA formation; and (4) enhanced dispersion by DA increases vulnerability to conduction block in our LQT2 rabbits. Our results implicate heterogeneous APD restitution in underlying arrhythmogenesis by increasing dispersion of repolarization through DA in this LQT model.

Comparison to other animal models of LQTS

Dispersion of repolarization has been implicated as an underlying mechanism of LQT-related arrhythmias in both previous pharmacological and transgenic animal models (Baker *et al.* 2000; Antzelevitch, 2001; Choi *et al.* 2002; Restivo *et al.* 2004; London *et al.* 2007; Brunner *et al.* 2008). I_{kr} blockade using E4031 increases APD gradient mostly between the apex and base (Choi *et al.* 2002). Transmural APD dispersion has been well described in the canine model using sotalol (Shimizu & Antzelevitch, 1999). Our data using a transgenic rabbit model corroborate dispersion of repolarization as a major contributor to arrhythmogenesis, yet add additional understanding of how dynamic repolarization in LQT2 increases dispersion via DA.

A transgenic model of Long QT syndrome has been previously developed in mice. The mouse model also provided insights into the relationship of APD dispersion and vulnerability to arrhythmias with programmed stimulation. However, mouse models have several well-known limitations: (1) a triangular shape of action potentials, lacking a plateau phase, (2) different repolarization kinetics, (3) difficulties in VF induction, and (4) lack of spontaneous sudden death. Therefore, the extrapolation of experimental results obtained from transgenic mice to human disease has been received

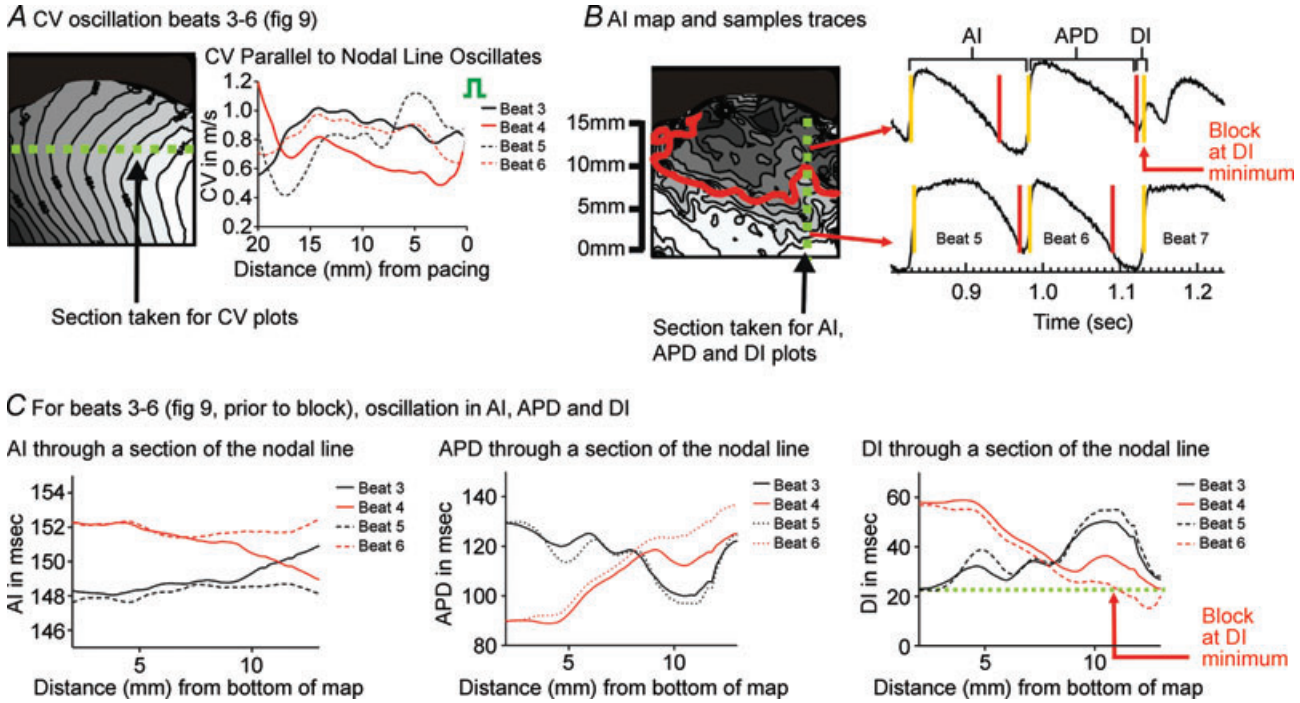

Figure 10. Detailed analysis of CV, AI, APD and DI in beats preceding conduction block formation in Fig. 9

A, activation map prior to the conduction block in Fig. 9*B*. The beat-to-beat changes of CVs along the green dashed line are shown in the right panel. *B*, repolarization map from Fig. 9*B*. AI, APD and DI measurements from beats 3–6 were taken along the dashed green line which transects the major nodal line (red). To the right of the map, traces of beats 5–7 are shown from above and below the nodal line with activation (yellow line) and repolarization (red line) marked. *C*, AI, APD and DI plots for beats 3–6 along dashed green line in the *B*. Note amplification of APD and DI oscillation at >10 mm from bottom. Conduction block occurred at the location of nadir of DI.

© 2009 The Authors. Journal compilation © 2009 The Physiological Society

with caution. The transgenic rabbit model of LQT2 used here has several advantages: (1) a rectangular shape of action potentials with plateau phase, (2) I_{Kr} and I_{Ks} delayed rectifiers (Vermeulen *et al.* 1994; Brunner *et al.* 2008), and (3) a sufficiently large heart size to maintain VT/VFs (Manoach *et al.* 1980; Banville & Gray, 2002). In addition, this transgenic LQT model showed sudden death due to spontaneous ventricular arrhythmias (Brunner *et al.* 2008), and early afterdepolarizations triggered with sympathetic stimulation (Ziv *et al.* 2008). In this investigation, LQT2 rabbits exhibited a high incidence of APD alternans which was spatially out of phase (discordant) and an increased incidence of VT/VF during our standard ramp stimulation protocol. This additional finding highlights the advantages of the transgenic rabbit models.

Increase of dispersion of repolarization by discordant alternans

Spatially discordant alternans was first described by Gilmore *et al.* (1967) with discordant RV and LV pulsus alternans in the dog. Since then, discordant APD alternans has emerged as an important factor that increases dispersion of repolarization dynamically and provides a substrate for reentry (Pastore *et al.* 1999; Qu *et al.* 2000; Clusin, 2003; Laurita *et al.* 2003; Pruvot *et al.* 2004; Goldhaber *et al.* 2005; Sato *et al.* 2007; Wilson & Rosenbaum, 2007; Wilson *et al.* 2009). However, its potential involvement in LQT related arrhythmias was not clearly understood. Our data from the transgenic rabbit model show multiple phases of dispersion in the LQT2 rabbits as change in heart rate is introduced: (phase 1) dispersion initially decreases with small increases in heart rate due to APD shortening; (phase 2) at faster heart rates, heterogeneity in restitution slopes is responsible for increase in APD dispersion, and this increase is bimodal, with an initial slow rise due to regional variability in APD oscillations when concordant alternans is initiated and an acceleration in rise of dispersion with onset of DA, and the formation of a nodal line; (phase 3) dispersion begins to diminish at very short CLs near refractoriness due to occurrence of multiple beat-to-beat changes in nodal lines (see Fig. 4). Our data strongly suggest that DA in this LQT2 animal model enhances dispersion and increases vulnerability to reentry formation.

Mechanisms underlying DA in transgenic rabbit model of LQT2

DA can potentially arise from multiple recognized mechanisms (Echebarria & Karma, 2007; Garfinkel, 2007; Wilson & Rosenbaum, 2007). CV restitution can lead to discordant alternans through beat-to-beat differences in activation intervals at regions close to and far from a pacing site. Alternatively, sufficient tissue heterogeneity can result in out of phase beat-to-beat alternation of APD with introduction of a premature beat or shortened pacing CL (Yue *et al.* 2005; Nash *et al.* 2006; Pastore *et al.* 2006; Echebarria & Karma, 2007; Keldermann *et al.* 2008). Such a change in stimulation results in two cardiac regions with a disparate DI–APD response due to disparate APD restitution curves. In this investigation, we present for the first time a detailed analysis of the contribution of these two potential mechanisms to the onset and behaviour of DA in a transgenic rabbit model of LQT2 and controls. Our model demonstrates that early DA arises even at physiological heart rates in LQT2 and this early onset is well correlated with dispersion of APD and its restitution. The onset of DA at physiological heart rates underscores the potential for DA to be an important mechanism of arrhythmogenesis *in vivo*. In contrast, DA in LMCs was dependent on beat-to-beat CV oscillations. Therefore, DA in LMCs requires that pacing occurs at intervals within relative refractoriness. Thus, shorter pacing CLs are required in LMCs compared to LQT2s. It is important to note that in the LMC case, our AI plots through regions of DA do not exactly reproduce the predicted behaviour from modelling studies, where AI maximum oscillation coincides with APD nodal line. In our case, near the APD nodal line, AI oscillation is attenuated. This attenuation was due to the sudden CV acceleration on even beats (Fig. 4*C*, red) and loss of beat-to-beat CV oscillation. The sudden CV acceleration may be due to transmural conduction, perhaps via Purkinje/endocardial activation. Alternatively anisotropic conduction along fibre orientation may allow for acceleration of CV via spatially heterogeneous CV restitution. Further studies, including transmural preparations are required to investigate these possibilities.

Complex nodal line behaviour at short CLs

Interestingly, as we pace LQT2 hearts at shorter CLs, close to tissue refractoriness, CV restitution begins to contribute to nodal line formation as well. The result is a dynamically shifting nodal line pattern associated with conduction block formation. Unstable nodal lines were also reported to exist in the rabbit as a result of slow APD accommodation termed 'cardiac short-term memory' (Mironov *et al.* 2008). The nodal lines in LQT2 rabbits, however, persist in shifting beyond the initial 10 s post-change in pacing CL, suggesting the phenomenon is less likely to be due to cardiac memory. Furthermore, at pacing CLs shorter than 160 ms, our LQT2 nodal lines demonstrate congruence with both activation and regions of transition in heterogeneity – namely divisions in APD dispersion across the mapped surface.

The simultaneous contribution of different DA mechanisms may increase vulnerability to reentry

© 2009 The Authors. Journal compilation © 2009 The Physiological Society

formation by multiple mechanisms. First, as shown, CV oscillations that may produce DA in homogeneous tissue in the LMC result in APD dispersion amplification when present in heterogeneous tissue in LQT2. Furthermore, the resulting conduction block generates large shifts in nodal lines. As a result, there is an increasing number of nodal lines (where the gradient of repolarization is greatest), and complex shifts in repolarization gradients. In such a case, the probability of propagating waves encountering a large repolarization gradient will be increased, resulting in higher likelihood of unidirectional conduction block. It would be interesting to further study which combinations of CV oscillations or APD dispersion has a greater propensity for formation of unidirectional conduction block and reentry when the two co-exist. It is important to point out that in 3 of the 5 LQT2 hearts studied, VF was triggered even before nodal lines due to CV alternation actually occurred. Although the case number is limited ($n = 2$ out of 5), when CV and APD dispersion nodal lines co-exist, our maps of conduction block formation demonstrate the occurrence of block parallel to nodal lines caused by APD dispersion. These points suggest that significant APD dispersion in this model plays an important role in enhancement of dispersion and arrhythmogenesis via formation of discordant alternans.

Mechanisms underlying APD dispersion

The underlying cause of tissue heterogeneity and dispersion of APD in LQT2 rabbits is not clear. Since LQT2 genotypes lack I_{Kr}, one can postulate that heterogeneous expression of remaining I_{Ks} may play a dominant role in the repolarization gradient. In a drug induced LQT2 model using an I_{Kr} blocker (E4031), a huge apex-to-base APD gradient was observed (Choi *et al.* 2002), in line with voltage clamp studies that showed low I_{Ks}/I_{Kr} ratio at the apex compared to base in rabbit hearts (Cheng *et al.* 1999). Our transgenic model also showed enhanced dispersion compared to controls; but a smaller increase in dispersion and more complex epicardial dispersion pattern was seen compared to the systematic apex-to-base dispersion seen in the drug induced acute model of LQT2. These discrepancies may reflect genetic remodelling of various ion channels and related proteins that could potentially result from the loss of I_{Kr}. Further studies into the molecular mechanisms underlying APD heterogeneities in this model are warranted.

Clinical relevance of the study

As demonstrated in our LQT2 rabbit model, DA can occur due to combinations of competing mechanisms even in the same heart. It therefore follows that different test modalities may be necessary to cull out the propensity for DA (and arrhythmia) in patients with different underlying cardiac pathology. This may explain some of the disparate results from clinical research applying alternans recording (microvolt T-wave alternans) to the clinical field (Gehi *et al.* 2005; Narayan, 2006; Gold *et al.* 2006; Scheinman & Keung, 2008). Since APD dispersion rather than CV restitution was the governing factor at the onset of discordant alternans in this LQT2 model, one may expect that T-wave alternans, rather than QRS alternans would be an important predictor of sudden death in this specific population. Although microvolt T-wave alternans in a small mixed long QT genotypic population has been described (Nemec *et al.* 2003), a genotypic specific LQT2 investigation into the predictive value of microvolt T-wave alternans has yet to be performed.

Limitations

Our study involves triggering DA with epicardial pacing, which has been used in other whole heart investigations (Banville & Gray, 2002; Choi *et al.* 2007; Hayashi *et al.* 2007; Mironov *et al.* 2008). The relationship of DA that arises from this mode of pacing and native formation of DA due to triggered activity such as EADs in LQTS has not been fully elucidated. Our mapping was limited to the epicardial surface and does not include endocardial and transmural mapping. Due to the limited access to female transgenic rabbits for breeding, we focused on male transgenic rabbits. Sex differences in arrhythmia mechanisms in this transgenic model may need further investigation.

Our transgenic LQT2 rabbit model mimics the arrhythmia phenotype seen in LQT2 patients with spontaneous polymorphic VT associated with the 'short–long–short' pattern, 'R on T' premature beats in free moving animals (Brunner *et al.* 2008). However, the repolarization patterns seen in this *ex vivo* study may not recapitulate those seen in LQT2 human myocardium. Furthermore, the mechanisms responsible for the abnormal repolarization observed in this model are unknown. Therefore, the generalization of these data to normal or diseased myocardium should be done with great caution.

Conclusions

For the first time, we demonstrate the importance of tissue spatial heterogeneity in the formation of DA and vulnerability to reentrant arrhythmias in a transgenic rabbit LQT2 model. The underlying molecular cause of tissue heterogeneity and dispersion of APD in LQT2 rabbits is not clear and warrants further investigation. In addition, our data suggest that competing contributions from tissue heterogeneity and CV restitution at shorter

© 2009 The Authors. Journal compilation © 2009 The Physiological Society

cycle length pacing results in chaotic nodal line shifts, which are associated with formation of conduction block possibly facilitating reentry formation and VF in this animal model. Our study underscores the potential importance of different mechanisms and possibly multiple mechanisms in the formation of DA in a single pathological substrate, which may augment the risk of arrhythmia.

References

Antzelevitch C (2001). Molecular biology and cellular mechanisms of Brugada and long QT syndromes in infants and young children. *J Electrocardiol* **34**(Suppl), 177–181.

Antzelevitch C (2007). Ionic, molecular, and cellular bases of QT-interval prolongation and torsade de pointes. *Europace* **9**(Suppl 4), iv4–15.

Baker LC, London B, Choi BR, Koren G & Salama G (2000). Enhanced dispersion of repolarization and refractoriness in transgenic mouse hearts promotes reentrant ventricular tachycardia. *Circ Res* **86**, 396–407.

Banville I & Gray RA (2002). Effect of action potential duration and conduction velocity restitution and their spatial dispersion on alternans and the stability of arrhythmias. *J Cardiovasc Electrophysiol* **13**, 1141–1149.

Bishop MJ, Gavaghan DJ, Trayanova NA & Rodriguez B (2007*a*). Photon scattering effects in optical mapping of propagation and arrhythmogenesis in the heart. *J Electrocardiol* **40**, S75–80.

Bishop MJ, Rodriguez B, Qu F, Efimov IR, Gavaghan DJ & Trayanova NA (2007*b*). The role of photon scattering in optical signal distortion during arrhythmia and defibrillation. *Biophys J* **93**, 3714–3726.

Bray MA & Wikswo JP (2003). Examination of optical depth effects on fluorescence imaging of cardiac propagation. *Biophys J* **85**, 4134–4145.

Brunner M, Peng X, Liu GX, Ren XQ, Ziv O, Choi BR, Mathur R, Hajjiri M, Odening KE, Steinberg E, Folco EJ, Pringa E, Centracchio J, Macharzina RR, Donahay T, Schofield L, Rana N, Kirk M, Mitchell GF, Poppas A, Zehender M & Koren G (2008). Mechanisms of cardiac arrhythmias and sudden death in transgenic rabbits with long QT syndrome. *J Clin Invest* **118**, 2246–2259.

Cheng J, Kamiya K, Liu W, Tsuji Y, Toyama J & Kodama I (1999). Heterogeneous distribution of the two components of delayed rectifier K^+ current: a potential mechanism of the proarrhythmic effects of methanesulfonanilide class III agents. *Cardiovasc Res* **43**, 135–147.

Chinushi M, Kozhevnikov D, Caref EB, Restivo M & El-Sherif N (2003). Mechanism of discordant T wave alternans in the in vivo heart. *J Cardiovasc Electrophysiol* **14**, 632–638.

Choi BR, Burton F & Salama G (2002). Cytosolic Ca^{2+} triggers early afterdepolarizations and Torsade de Pointes in rabbit hearts with type 2 long QT syndrome. *J Physiol* **543**, 615–631.

Choi BR, Jang W & Salama G (2007). Spatially discordant voltage alternans cause wavebreaks in ventricular fibrillation. *Heart Rhythm* **4**, 1057–1068.

Clusin WT (2003). Calcium and cardiac arrhythmias: DADs, EADs, and alternans. *Crit Rev Clin Lab Sci* **40**, 337–375.

Dessertenne F (1966). La tachycardie ventricularire à deux foyers opposés variables. *Arch Mal Coeur* **59**, 263–272.

Drummond GB (2009). Reporting ethical matters in *The Journal of Physiology*: standards and advice. *J Physiol* **587**, 713–719.

Echebarria B & Karma A (2007). Mechanisms for initiation of cardiac discordant alternans. *Eur Phys J Special Topics* **146**, 217–231.

Efimov IR, Huang DT, Rendt JM & Salama G (1994). Optical mapping of repolarization and refractoriness from intact hearts. *Circulation* **90**, 1469–1480.

El-Sherif N & Turitto G (1999). The long QT syndrome and torsade de pointes. *Pacing Clin Electrophysiol* **22**, 91–110.

Fagundes ML, Maia IG, Cruz FE, Alves PA, Boghossian SH, Ribeiro JC & Sa R (2000). Arrhythmogenic cardiomyopathy of the right ventricle. Predictive value of QT interval dispersion to assess arrhythmogenic risk and sudden death. *Arq Bras Cardiol* **75**, 115–124.

Fedorov V, Lozinsky I, Sosunov E, Anyukhovsky E, Rosen M, Balke C & Efimov I (2007). Application of blebbistatin as an excitation-contraction uncoupler for electrophysiologic study of rat and rabbit hearts. *Heart Rhythm* **4**, 619–626.

Garfinkel A (2007). Eight (or more) kinds of alternans. *J Electrocardiol* **40**, S70–74.

Gehi AK, Stein RH, Metz LD & Gomes JA (2005). Microvolt T-wave alternans for the risk stratification of ventricular tachyarrhythmic events: a meta-analysis. *J Am Coll Cardiol* **46**, 75–82.

Gettes LS & Reuter H (1974). Slow recovery from inactivation of inward currents in mammalian myocardial fibres. *J Physiol* **240**, 703–724.

Gilmore JP, Powell WJ, Graham TP & Clancy RL (1967). Discordant pulsus alternans in dog heart. *Am J Physiol* **212**, 1515–1518.

Gold MR, Ensley D, Chilson D, Ip JH, Costantini O, Bloomfield D, Poole JE, McNulty SE, Lee K, Bardy GH (2006). T-wave alternans SCD HeFT Study: Primary endpoint analysis. *Circulation* **114**(Suppl), 428.

Goldhaber JI, Xie LH, Duong T, Motter C, Khuu K & Weiss JN (2005). Action potential duration restitution and alternans in rabbit ventricular myocytes: the key role of intracellular calcium cycling. *Circ Res* **96**, 459–466.

Hayashi H, Shiferaw Y, Sato D, Nihei M, Lin SF, Chen PS, Garfinkel A, Weiss JN & Qu Z (2007). Dynamic origin of spatially discordant alternans in cardiac tissue. *Biophys J* **92**, 448–460.

Jammalamadaka S & SenGupta A (2001). *Topics in Circular Statistcs*. World Scientific Press, Singapore.

Keldermann RH, ten Tusscher KH, Nash MP, Hren R, Taggart P & Panfilov AV (2008). Effect of heterogeneous APD restitution on VF organization in a model of the human ventricles. *Am J Physiol Heart Circ Physiol* **294**, H764–774.

Laurita KR, Katra R, Wible B, Wan X & Koo MH (2003). Transmural heterogeneity of calcium handling in canine. *Circ Res* **92**, 668–675.

Liu J & Laurita KR (2005). The mechanism of pause-induced torsade de pointes in long QT syndrome. *J Cardiovasc Electrophysiol* **16**, 981–987.

© 2009 The Authors. Journal compilation © 2009 The Physiological Society

London B, Baker LC, Petkova-Kirova P, Nerbonne JM, Choi BR & Salama G (2007). Dispersion of repolarization and refractoriness are determinants of arrhythmia phenotype in transgenic mice with long QT. *J Physiol* **578**, 115–129.

Manoach M, Netz H, Erez M & Weinstock M (1980). Ventricular self-defibrillation in mammals: age and drug dependence. *Age Ageing* **9**, 112–116.

Mironov S, Jalife J & Tolkacheva EG (2008). Role of conduction velocity restitution and short-term memory in the development of action potential duration alternans in isolated rabbit hearts. *Circulation* **118**, 17–25.

Mironov SF, Vetter FJ & Pertsov AM (2006). Fluorescence imaging of cardiac propagation: spectral properties and filtering of optical action potentials. *Am J Physiol Heart Circ Physiol* **291**, H327–335.

Morita H, Wu J & Zipes DP (2008). The QT syndromes: long and short. *Lancet* **372**, 750–763.

Narayan SM (2006). T-wave alternans and the susceptibility to ventricular arrhythmias. *J Am Coll Cardiol* **47**, 269–281.

Nash MP, Bradley CP, Sutton PM, Clayton RH, Kallis P, Hayward MP, Paterson DJ & Taggart P (2006). Whole heart action potential duration restitution properties in cardiac patients: a combined clinical and modelling study. *Exp Physiol* **91**, 339–354.

Nemec J, Ackerman MJ, Tester DJ, Hejlik J & Shen WK (2003). Catecholamine-provoked microvoltage T wave alternans in genotyped long QT syndrome. *Pacing Clin Electrophysiol* **26**, 1660–1667.

Nishida Y, Chen QH, Zhou MS & Horiuchi J (2002). Sinoaortic denervation abolishes pressure resetting for daily physical activity in rabbits. *Am J Physiol Regul Integr Comp Physiol* **282**, R649–657.

Odening KE, Hyder O, Chaves L, Schofield L, Brunner M, Kirk M, Zehender M, Peng X & Koren G (2008). Pharmacogenomics of anesthetic drugs in transgenic LQT1 and LQT2 rabbits reveal genotype-specific differential effects on cardiac repolarization. *Am J Physiol Heart Circ Physiol* **295**, H2264–2272.

Pastore JM, Girouard SD, Laurita KR, Akar FG & Rosenbaum DS (1999). Mechanism linking T-wave alternans to the genesis of cardiac fibrillation. *Circulation* **99**, 1385–1394.

Pastore JM, Laurita KR & Rosenbaum DS (2006). Importance of spatiotemporal heterogeneity of cellular restitution in mechanism of arrhythmogenic discordant alternans. *Heart Rhythm* **3**, 711–719.

Pertsov AM, Zemlin CW, Hyatt CJ & Bernus O (2006). What can we learn from the optically recorded epicardial action potential? *Biophys J* **91**, 3959–3960.

Pruvot EJ, Katra RP, Rosenbaum DS & Laurita KR (2004). Role of calcium cycling *versus* restitution in the mechanism of repolarization alternans. *Circ Res* **94**, 1083–1090.

Qu Z, Garfinkel A, Chen PS & Weiss JN (2000). Mechanisms of discordant alternans and induction of reentry in simulated cardiac tissue. *Circulation* **102**, 1664–1670.

Restivo M, Caref EB, Kozhevnikov DO & El-Sherif N (2004). Spatial dispersion of repolarization is a key factor in the arrhythmogenicity of long QT syndrome. *J Cardiovasc Electrophysiol* **15**, 323–331.

Saenen JB & Vrints CJ (2008). Molecular aspects of the congenital and acquired long QT syndrome: clinical implications. *J Mol Cell Cardiol* **44**, 633–646.

Sato D, Shiferaw Y, Qu Z, Garfinkel A, Weiss JN & Karma A (2007). Inferring the cellular origin of voltage and calcium alternans from the spatial scales of phase reversal during discordant alternans. *Biophys J* **92**, L33–35.

Sauer AJ, Moss AJ, McNitt S, Peterson DR, Zareba W, Robinson JL, Qi M, Goldenberg I, Hobbs JB, Ackerman MJ, Benhorin J, Hall WJ, Kaufman ES, Locati EH, Napolitano C, Priori SG, Schwartz PJ, Towbin JA, Vincent GM & Zhang L (2007). Long QT syndrome in adults. *J Am Coll Cardiol* **49**, 329–337.

Scheinman MM & Keung E (2008). The year in review of clinical cardiac electrophysiology. *J Am Coll Cardiol* **51**, 2075–2081.

Schwartz PJ (2006). The congenital long QT syndromes from genotype to phenotype: clinical implications. *J Intern Med* **259**, 39–47.

Schwartz PJ & Malliani A (1975). Electrical alternation of the T-wave: clinical and experimental evidence of its relationship with the sympathetic nervous system and with the long Q-T syndrome. *Am Heart J* **89**, 45–50.

Schwartz PJ, Periti M & Malliani A (1975). The long Q-T syndrome. *Am Heart J* **89**, 378–390.

Shimizu W & Antzelevitch C (1999). Cellular basis for long QT, transmural dispersion of repolarization, and torsade de pointes in the long QT syndrome. *J Electrocardiol* **32**(Suppl), 177–184.

Vermeulen JT, McGuire MA, Opthof T, Coronel R, de Bakker JM, Klopping C & Janse MJ (1994). Triggered activity and automaticity in ventricular trabeculae of failing human and rabbit hearts. *Cardiovasc Res* **28**, 1547–1554.

Watanabe MA, Fenton FH, Evans SJ, Hastings HM & Karma A (2001). Mechanisms for discordant alternans. *J Cardiovasc Electrophysiol* **12**, 196–206.

Webster G & Berul CI (2008). Congenital long-QT syndromes: a clinical and genetic update from infancy through adulthood. *Trends Cardiovasc Med* **18**, 216–224.

Weiss JN, Karma A, Shiferaw Y, Chen PS, Garfinkel A & Qu Z (2006). From pulsus to pulseless: the saga of cardiac alternans. *Circ Res* **98**, 1244–1253.

Wilson LD, Jeyaraj D, Wan X, Hoeker GS, Said TH, Gittinger M, Laurita KR & Rosenbaum DS (2009). Heart failure enhances susceptibility to arrhythmogenic cardiac alternans. *Heart Rhythm* **6**, 251–259.

Wilson LD & Rosenbaum DS (2007). Mechanisms of arrythmogenic cardiac alternans. *Europace* **9**(Suppl 6), vi77–82.

Yue AM, Franz MR, Roberts PR & Morgan JM (2005). Global endocardial electrical restitution in human right and left ventricles determined by noncontact mapping. *J Am Coll Cardiol* **46**, 1067–1075.

Zareba W, Moss AJ, le Cessie S & Hall WJ (1994). T wave alternans in idiopathic long QT syndrome. *J Am Coll Cardiol* **23**, 1541–1546.

© 2009 The Authors. Journal compilation © 2009 The Physiological Society

Ziv O, Odening KE, Kirk M, Brunner M, Schofield L, Chaves L, Zehender M, Peng X, Morales E, Koren G & Choi BR (2008). Sympathetic stimulation initiates dynamic triggered activity that degenerates into pVT and VF in LQT1 rabbits. *Circulation* **118**, 530.

Author contributions

O.Z., G.K. and B.-R.C.: conception, design, analysis and interpretation of data, drafting the article and revising it, and final approval of the version to be published. A.K.: design, interpretation of data, revision of the article, and final approval of the version to be published. A.E.B.: interpretation of data, revision of the article, and final approval of the version to be published. E.M.: analysis of data, revision of the article, and final approval of the version to be published. K.E.O.: screen of genotypes, interpretation of data, revision of the article, and final approval of the version to be published. X.P.: generation of transgenic rabbits and littermate controls. Y-k.S.: development of optical apparatus, development of data analysis algorithms as well as analysis of data, and final approval of the version to be published. All experiments were done at Cardiovascular Research Center, Rhode Island Hospital, Warren Alpert Medical School of Brown University, Providence, RI, USA.

Acknowledgements

The authors would like to thank Lorraine Schofield, Patricia Mastrofrancesco and Lenny Chaves for their dedicated administrative and animal care support. B.-R.C. and G.K. were supported by NIH grant RO1 HL046005-14. O.Z. was supported by American Heart Association Postdoctural Fellowship grant no. 0825980D.

© 2009 The Authors. Journal compilation © 2009 The Physiological Society